An Excitatory Neural Network Model of Spontaneous Activity in Developing Spinal Cord Using Synaptic Depression

Boris Vladimirski *
Courant Institute of Mathematical Sciences, New York University, New York, NY 10003

Joel Tabak
Michael J. O'Donovan
Laboratory of Neural Control, National Institute of Neurological Diseases and Stroke
National Institutes of Health, Bethesda, MD 20892

John Rinzel
Center for Neural Science and Courant Institute of Mathematical Sciences
New York University, New York, NY 10003

1 Introduction

Spontaneous activity produced by networks of synaptic connections is a characteristic feature of the developing nervous system. It has been reported in many different regions ([1]), including the hippocampus, retina, and the spinal cord, on which we concentrate in the current paper. Despite the ubiquitous character of this phenomenon, the underlying mechanisms are poorly understood. It is known ([1]), however, that developing networks are hyperexcitable, partly due to the fact that both GABA and glycine are functionally depolarizing at the prenatal stage. This work was inspired by the research done by Tabak et al. ([2]) and, in particular, is based on the same experimental data from the isolated lumbosacral spinal cord of the chick embryo. This preparation generates spontaneous episodes of activity (duration 5-90 sec, cycle duration 0.1-2 Hz) separated by much longer quiescent phases (2-30 min). It has been proposed ([4] and [1]) that the occurrence of episodes is a population phenomenon controlled by some form of activity-dependent network depression. On the basis of these experimental data, Tabak et al. have introduced a general firing-rate model of network activity in the form of a system of three coupled ODE's that incorporate two different depression time scales: a slow one, responsible for the termination of the episode and then the recovery from the quiescent phase, and a fast one, responsible for cycling within the episode. With this model, the authors have achieved qualitative agreement with the experimental data, including the developmental changes in the duration of episodes and inter-episode intervals. They also noted in their conclusions that their synaptic depression model was in better correspondence with the experimental data than their model based on cellular threshold adaptation. Parts of this work have been presented at the CNS meeting in 1999 ([3]).

However, despite its generality, the activity model of Tabak et al. was not cell-based; hence, its connection to biology remained unclear. In particular, there are some questions for which their mean-field model is inapplicable or difficult to interpret, such as the neuronal mechanisms that would produce the desired behavior, spatial structure in the network, relationship between that model's parameters and experimentally measured ones, etc. The current work attempts to model the spiking activity of a heterogeneous population of individual neurons directly using an n-cell network of leaky integrate-and-fire neurons with synaptic depression. As we show below, this network reproduces many, but currently not all, aspects of the experimentally observed behavior while maintaining a closer relation to underlying neurobiology.

*Correspondence should be addressed to Boris Vladimirski at the address above. E-mail: vladimir@cims.nyu.edu

2 Methods

The equations of this network model are:

$$\begin{aligned} \tau \dot{V}_i &= -V_i + I_i^{app} - (V_i - V_{syn}) g_{syn} \\ \dot{s}_i &= \alpha_s(t)(1 - s_i) - \beta_s s_i \\ \dot{d}_i &= \alpha_d(1 - d_i) - \beta_d(t) d_i \\ \dot{f}_i &= \alpha_f(1 - f_i) - \beta_f(t) f_i \end{aligned}$$

$$\text{Here } g_{syn} = \overline{g}_{syn} E^{-1}(A_i) \sum_{j \in A_i} s_j d_j f_j$$

If $V_i(t_i) = \Theta$, then $V_i = V_{reset}$ for all $t: \ t_i < t < t_i + r$, where Θ is a firing threshold, and r is the duration of the refractory period. τ is the membrane time constant, I_i^{app} is an applied current to neuron i supplied by sources outside of the network. We assume that the synaptic current to each neuron flows through such ionic channels that can be combined into one equivalent channel with a linear $i - v$ relationship, for which $\overline{g}_{syn}$ is the maximum synaptic conductance, and V_{syn} is the (constant) reversal potential. A_i is a set consisting of the indices of all neurons that make synapses on neuron i and $E(A_i) = n \cdot CP$ is the expected number of elements in A_i (CP is the probability that a randomly chosen two neurons are connected). s_i is the activity-dependent synaptic activation (gating variable) of all connections that neuron i makes on other neurons in the network. In its full generality and computer implementation, the model actually allows for probabilistic neurotransmitter release for each synapse originating at the same neuron and thus for a separate effective spiking history for each synapse. However, we do not utilize this possibility in the current work. d_i and f_i are, respectively, the activity-dependent slow and fast synaptic depression of all connections that neuron i makes on the other neurons in the network. β_s, α_d, and α_f are nonnegative constant rates of synaptic decay, slow depression recovery, and fast depression recovery.

$$\alpha_s(t) = \begin{cases} \alpha_s^c & \text{if } t - t_i < SAD \\ 0 & \text{otherwise} \end{cases}$$

Here α_s^c is a nonnegative constant, t_i is the time of the last spike of neuron i, and SAD is another nonnegative constant determining the time scale of synaptic activation, i.e., ionic channels opening. Once SAD time units have elapsed, the synaptic conductance decays exponentially to 0 at rate β_s. Similarly,

$$\beta_d(t) = \begin{cases} \beta_d^c & \text{if } t - t_i < DAD_d \\ 0 & \text{otherwise} \end{cases}$$

$$\beta_f(t) = \begin{cases} \beta_f^c & \text{if } t - t_i < DAD_f \\ 0 & \text{otherwise} \end{cases}$$

The parameter values that remained unchanged in all simulations were as follows (after normalization with respect to the membrane time constant; originally, $\tau = 20$ ms): $\tau = 1$, $\Theta = 1$, $V_{reset} = 0$, $r = 0.25$, $V_{syn} = 5$, $\alpha_s^c = 10$, $\beta_s = 1$, $SAD = DAD_d = DAD_f = 0.1$. All parameter values were chosen using available experimental data in such a way that the relative time scales of all dynamic processes and the range of firing rates remained similar to the biological ones (the parameter values are also similar to those used independently by Loebel and Tsodyks ([5]). n varied from 30 to 1000, and the distributions of applied currents included a uniform distribution below the threshold, a uniform distribution containing the threshold, and a bimodal uniform distribution. In the latter two cases, no more than 1/6 of the whole population had their applied currents set above the threshold and, thus, was active in the absence of any synaptic input.

Most of the numerical simulations were performed using a software package developed by Boris Vladimirski in C++. To solve the equations, the standard 4-step 4th-order Runge-Kutta method was used with the time step of 0.01. All the input and output to the package are provided through a set of text files, and the output was processed and visualized using Matlab. Matlab was also used to solve the consistency equation described below for a mean-field model of the network firing rate. Special attention was paid to the verification of the results using various network sizes, smaller time steps, etc. For smaller network sizes ($n \leq 50$), xpp was also used to confirm the validity of the results.

3 Results

3.1 Bistability with all depression variables frozen

Here we consider the network with spike-driven synaptic conductances only; both fast and slow depression are absent ($d_i = f_i = 1$ for all neurons and times). A basic feature of Tabak et al. was bistability between a low and a high firing rate steady states on the fast time scale. This bistability was induced by the recurrent excitation in the network coupled with a proper choice of the parameters. With the introduction of a slow synaptic depression, the two states would alternate on a slow time scale leading to slow episodic behavior. Similarly,

we first attempt to find bistability between a stable low-activity steady state and a stable high-activity steady state for a range of $\overline{g}_{syn}$-values in the current spiking network. It could then serve as a basis for slow episodic behavior. Note that both the experimental data and the model of Tabak et al. are specified in terms of average firing rate across the network, not the spiking of individual neurons. Hence, we need a corresponding measure for this model to enable us to compare our findings with theirs.

3.1.1 Derivation of a mean-field model

We use the instantaneous mean (across the population) firing rate (MFR) as a measure of network activity and develop an *ad hoc* analytical mean-field model to facilitate the analysis of the steady-state dependence of the MFR on $\overline{g}_{syn}$. This derivation is based on the following assumptions:

1. The synaptic input to each neuron is the same for all neurons. In particular, we assume that the network is fully-connected and that there is no stochastic release: $A_i = \{1,\ 2, \ldots,\ n\}$, and $E(A_i) = n$ for all i. We believe that the latter two assumptions can be lifted if A_i's are identically chosen samples from the same distribution for all i, and $E(A_i)$ is large enough (e.g., $E(A_i) \geq 50$).

2. The synaptic input to each neuron is constant in time. This is reasonable if all neurons are firing asynchronously, which we expect to be the case due to the heterogeneity imparted by applied currents.

3. This constant input can be obtained by replacing the synaptic conductances by their temporally averaged values. This is reasonable if the MFR of the firing subpopulation is sufficiently high.

Denoting this constant network-driven synaptic conductance by $g_{syn} = \overline{g}_{syn} n^{-1} \sum_{j=1}^{n} s_j$, we compute the frequency of firing for each neuron i as a function of g_{syn}. Then, we compute the average synaptic conductance for each synapse and recompute g_{syn} following our assumptions. This gives us a self-consistency equation for g_{syn}. In the limit of large n, we can replace the discrete average over the population by its continuous analog to obtain the following general self-consistency condition:

$$g_{syn} = \overline{g}_{syn} \int_{-\infty}^{\infty} h(I) \tilde{s}(I,\ g_{syn}) dI$$

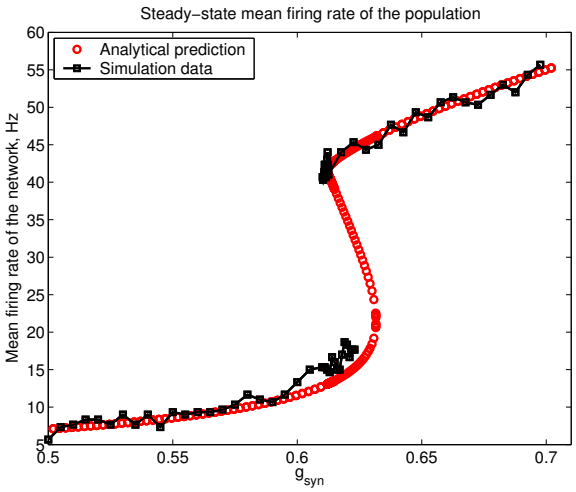

Figure 1: Steady-state firing rates for the uniform distribution of I_{app} on [0; 1.2]. Analytical predictions are shown in red, simulation results (all for $n = 50$) in black. Fig. 1 shows the bifurcation diagram of the network firing rate vs. $\overline{g}_{syn}$, which demonstrates the desired bistability and good correspondence between the numerical results and the analytical predictions. The intermediate branch is not seen in simulations and thus is conjectured to be unstable. This is true for 2A and 2B below as well.

Here $h(I)$ is the probability density function of the distribution of applied currents and $\tilde{s}(I,\ g_{syn})$ is the temporal average of the synaptic gating variable driven by the neuron with applied current I and network synaptic conductance g_{syn}. This has been derived analytically following the strict periodicity assumption above and using the input-output relation for our neurons.

In qualitative terms, the averaging process described here is a double averaging, first, temporal, and then, across the population. The temporal averaging is done analytically for these synapses, but the population averaging, i.e., integration, has to be done numerically due to the highly nonlinear nature of $f(I,\ g_{syn})$. Finally, a numerical nonlinear equation solver has to be used to solve the consistency equation.

3.1.2 Numerical simulations

Some results of extensive numerical simulations and their comparison with the analytical predictions are shown in Fig. 1 and 2 (for 1 and 2A, $g_{syn} = \overline{g}_{syn}$ elsewhere in the text).

As these figures show, the n-cell network indeed

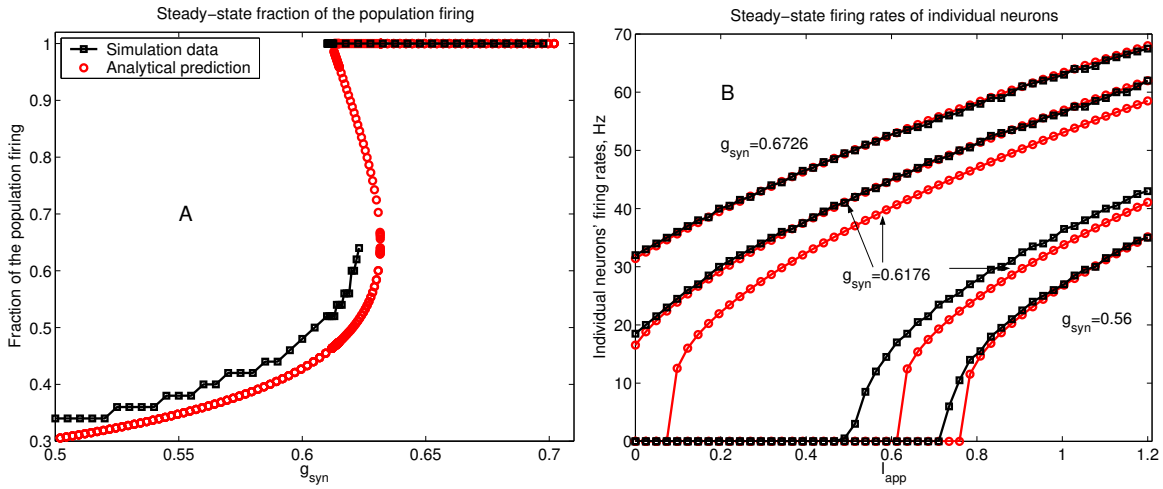

Figure 2: Steady-state firing rates for the uniform distribution of I_{app} on [0; 1.2]. Analytical predictions are shown in red, simulation results (all for $n = 50$) in black. 2A shows the bifurcation diagram of the fraction of the population firing vs. $\overline{g}_{syn}$. Note that the entire network is active on the upper branch, but not on the other two branches. The staircase-like structure of the simulation results in 1B is caused by the finite size of the network. 2B shows the steady-state profiles of the firing rates of the individual neurons for three different values of $\overline{g}_{syn}$. Note that for $\overline{g}_{syn} = 0.56$ and $\overline{g}_{syn} = 0.6726$, there is only one self-consistent g_{syn}-value, as predicted by Fig. 1, but for $\overline{g}_{syn} = 0.6176$, there are three self-consistent g_{syn}-values, and, correspondingly, three firing-rate profiles.

demonstrates the expected bistability between the two steady firing states for a range of $\overline{g}_{syn}$-values. Furthermore, the correspondence between the numerical results and the analytical predictions is good for both the network MFR and individual neurons' firing rates and it becomes perfect as n becomes larger and larger. The intermediate steady state, unlike the other two, is not seen in simulations due to, presumably, its unstable character, which is typical of such s-shaped input-output curves.

The narrower and slightly shifted bistability range for the simulation results in Fig. 1 is a finite size effect coupled with the sensitivity of the dynamical picture near the knees. Much better correspondence can be obtained by using large $n \geq 500$, but these would require too much computer time to produce the entire figure.

3.2 Introduction of slow depression: episodic behavior

Keeping the fast depression fixed at 1, we now activate the slow (compared to the voltage time scale) depression variables. It seems plausible to replace the combined effects of n individual slow depressions by their average to multiply $\overline{g}_{syn}$. Then, since this depression is slow compared to the voltage time scale, we would expect the trajectory to follow the bifurcation diagram obtained above and, thus, observe episodes of activity for a proper choice of the depression parameter values (the actual results are shown in Fig. 4). Indeed, as Fig. 3A shows, episodes are now observed in simulations. However, as Fig. 4 shows, the network MFR fails to follow the bifurcation diagram, especially, in the silent phase (inter-episode interval). Since in the silent phase most of the network is not active and hence their depressions tend to 1, as opposed to the endogeneously active neurons' depressions that are typically below 0.5, this is, perhaps, natural: even though the average population depression is high, there are only a few cells active, and their depressions are much lower. Hence, they, rather than the depression variables of the silent neurons, need to recover enough to recruit the rest of the population into an episode. Thus, the network remains in the silent phase for much higher values of the effective g_{syn} than the bifurcation diagram predicts. This discrepancy is very important in that it exemplifies the difference between the mean-field model and a heterogeneous population of spiking neurons. In the active phase, the depression distribution is much tighter except near the knee, where the simulation results diverge from the analytical prediction.

To understand the nature of this difference, let

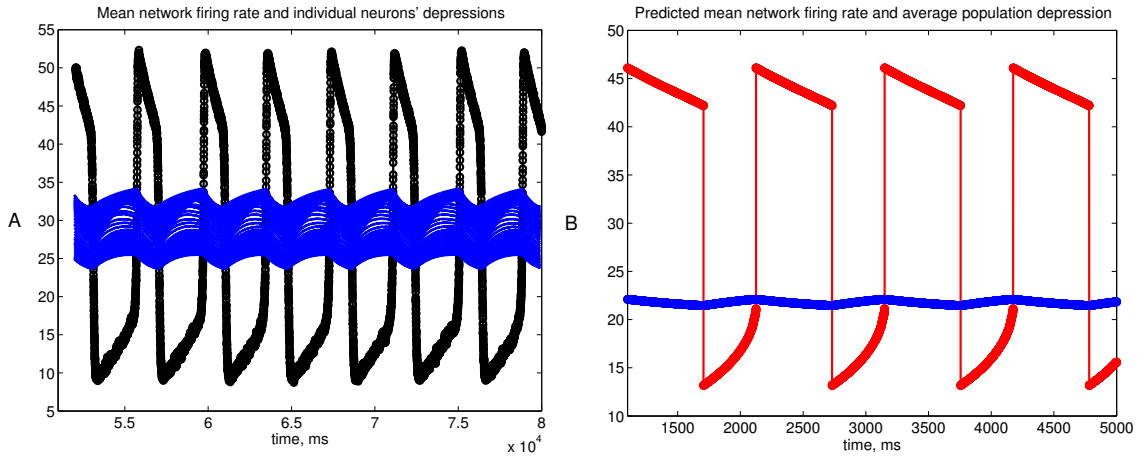

Figure 3: Episodic behavior for the uniform distribution of I_{app} on [0; 1.2], $\alpha_d = 0.01$, $\beta_d^c = 0.044$. Analytical predictions of the network firing rate are shown in red, depression variables in blue, simulation results (all for $n = 500$) in black. 3A shows a simulation-produced time course of the mean network firing rate that demonstrates episodes. Superimposed are individual neurons' depression variables (the scale for these is arbitrary). Note that all of the depression variables decay during an episode, and then recover during most of the silent phase. The separation between the active and the silent neurons is especially prominent during the silent phase. 3B corresponds to 3A, with the simulation data of 3A replaced by the analytical model consisting of one population average depression variable (shown in blue) and the analytical bifurcation diagram of Fig. 1. Note that even though the general shape is the same, the inter-episode period is shorter, the episode duration is longer relative to the total period of oscillations, and the mean firing rate slope is more shallow during an episode in 3B as compared with 3A.

us now examine the assumptions under which such averaging can be carried out:

$$\dot{d}_i = \alpha_d(1 - d_i) - \beta_d(t)d_i$$

1. Since the time scale of d_i is much slower than the one of V_i, we can replace $\beta_d(t)$ by its temporal average over a few periods to obtain $\dot{d}_i \approx \alpha_d(1 - d_i) - \beta_d^c DAD_d r_i d_i$, assuming $DAD_d < r$, where r_i is the current firing rate of neuron i.

2. Now, average d_i's instantaneously over the (sub)population: $\dot{d} = \alpha_d(1 - d) - \beta_d^c DAD_d \frac{1}{n}\sum_{i=1}^{n} r_i d_i \approx \alpha_d(1 - d) - \beta_d^c DAD_d r(t)d$, where d is the average slow depression across the population, and $r(t)$ is the instantaneous mean firing rate. The second equality here is the assumption that we make.

3. The final assumption is that we can replace $E^{-1}(A_i)\sum_{j\in A_i} s_j d_j$ by $d \cdot E^{-1}(A_i)\sum_{j\in A_i} s_j$.

Now we can use the ODE for d to obtain its nullcline in the $r - g_{syn}$ coordinates, where $g_{syn} = d \cdot \overline{g}_{syn}$.

In view of the discrepancy between the analytical bifurcation diagram and the simulation results shown in Fig. 4, let us develop a simple model of the network MFR. Since d is slow compared to the voltage or MFR time scale, a very simple model for the network MFR, then, consists of the analytical bifurcation diagram of Fig. 1 together with the ODE for d to compute the predicted network MFR time course (Fig. 3B; also, cf. Fig. 3A). This description has a substantial advantage of utilizing only one dynamic variable in addition to the bifurcation diagram that has already proved to be accurate so that phase-plane analysis can be used. However, even though the general shape of the time course in Fig. 3B is similar to that in Fig. 3A, many important details are different, as discussed in the caption of Fig. 3. As expected, this discrepancy agrees with the one demonstrated by the simulation results.

To correct for the deficiencies of depression averaging over the entire population, it seems to be much more promising to attempt to analyze this in terms of two populations of neurons, one that is firing and the other one that is not. The boundary between the two is, generally, a function of time, and we could expect this depression averaging to be valid within each population, but not across the two. Then, we can view the output from one population as an external input to the other, shifting its

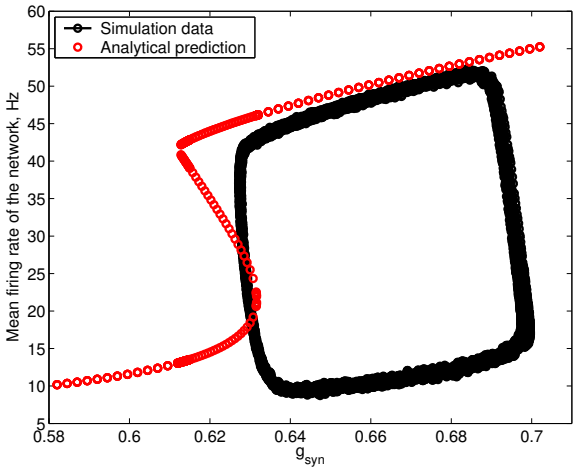

Figure 4: Episodic behavior for the uniform distribution of I_{app} on [0; 1.2], $\alpha_d = 0.01$, $\beta_d^c = 0.044$. Analytical predictions of the network firing rate are shown in red, depression variables in blue, simulation results (all for $n = 500$) in black. Fig. 4 shows a simulation-produced time course of the MFR superimposed on the analytical bifurcation diagram using $g_{syn} = d \cdot \overline{g}_{syn}$ as the slow x-axis variable, i.e., the effective maximum synaptic conductance (see the discussion in the text). It is especially important in that it demonstrates that the use of the population average depression does not lead to good agreement with the bifurcation diagram of Fig. 1, especially, during the silent phase.

nullclines, etc.

3.3 Episodes and cycling do not coexist in the current model

We are currently actively exploring the effects stemming from the introduction of the fast depression variables into the model. Preliminarily, we believe we have observed fast cycling with it. However, our preliminary numerical and analytical results seem to indicate that the current model is not capable of supporting both episodes and cycling for the same set of parameter values. We believe that it is the consequence of the form of the synaptic and depression ODE's used.

4 Future directions

1. Development of a biologically plausible model (perhaps, obtained by modifying the synaptic and depression ODE's appropriately) that does display both cycling and episodes simultaneously in an n-cell excitatory network.

2. Development of a qualitatively, if not quantitavely, correct analytical model via a mean-field or population density approaches.

3. Development of a more biologically realistic neuronal model to attempt to match the experimental data closely.

References

[1] O'Donovan M. (1999) The origin of spontaneous activity in developing networks of the vertebrate nervous system. Curr. Opin. Neurobiol. 9:94–104.

[2] Tabak J., Senn W., O'Donovan M., Rinzel J. (2000) Modeling of spontaneous activity in developing spinal cord using activity-dependent depression in an excitatory network. J. Neurosci. 20(8):3041–3056.

[3] Tabak J., Senn W., O'Donovan M., Rinzel J. (1999) Comparison of two models for pattern generation based on synaptic depression. Neurocomputing 26-27:551–556.

[4] O'Donovan M., Chub N. (1997) Population behavior and self-organization in the genesis of spontaneous rhythmic activity by developing spinal networks. Semin. Cell. Dev. Biol. 8:21–28.

[5] Loebel A., Tsodyks M. (2002) Computation by ensemble synchronization in recurrent networks with synaptic depression. J. Comput. Neurosci. 13:111–124.